Resonant Passive Mode-Locked Nd:YLF Laser

Ursula Keller, *Member, IEEE,* and T. Heng Chiu

Abstract—**Resonant passive mode locking (RPM) is a new coupled cavity mode-locking technique for solid-state lasers. We review the theory of RPM lasers and present experimental results of an improved Nd:YLF RPM laser that produced stable pulses as short as 3.7 ps at a repetition rate of 250 MHz. The average output power was 550 mW with 1.3 W average pump power from a Ti:sapphire laser. We were able to couple 85% out of the nonlinear coupled cavity and still maintain stable mode locking. In RPM an amplitude nonlinearity such as absorption bleaching in a semiconductor reflector introduces an intensity dependent reflectivity which strongly mode locks the laser. The reduced carrier lifetime in a low-temperature MBE-grown (LT) InGaAs–GaAs quantum-well reflector produces a sufficiently fast saturable absorber in the coupled cavity. The nonlinear semiconductor reflector has several key features for generating short pulses. It is self-starting, no active cavity length control is required, and the strength of the amplitude nonlinearity can be custom designed by the focusing lens, the absorber thickness, and band-gap engineering. In addition, the reflector is a compact device with a bulk nonlinearity that requires no critical alignment. One LT quantum-well reflector works for any repetition rate, limited at higher pulse repetition rates by the carrier lifetime.**

I. Introduction

THE recent renaissance in solid-state lasers due to diode pumping and new tunable materials has stimulated new mode-locking efforts for such lasers. Passive mode locking of solid-state lasers, such as rare earth and transition metal lasers, offered a new challenge because many dye laser mode-locking techniques do not work, due to a ≈ 1000 times smaller gain cross section. In Nd:YLF lasers the intracavity pulse energy density is typically much smaller than the saturation fluence. Therefore, no gain saturation is assisting a saturable absorber during the pulse formation process, and a "fast" saturable absorber is required. In the case of a "fast" saturable absorber the recovery time is comparable to the final pulse duration, and the dominant pulse forming process is controlled by the absorber.

Semiconductor saturable absorbers allow an all-solid-state ultrafast laser technology and have the advantage of being compact and of covering bandgaps from the visible to the infrared. Semiconductor saturable absorbers have been previously used to mode lock diode [1] and color center lasers [2], [3]. We will show in this paper that a "semi-fast" saturable absorber with a recovery time of 25 ps can produce pulse durations of only a few picosecond. A low-temperature MBE grown semiconductor can form such a "semi-fast" saturable absorber. The nonlinearity is based on absorption bleaching, where the absorption is first decreased by the carriers generated within one laser pulse, and then increased by carrier recombination. The carrier recombination time, and therefore the recovery time of the saturable absorber, is significantly reduced using low-temperature MBE growth. Unfortunately, such a saturable absorber would introduce too much loss inside a Nd:YLF laser. A coupled cavity mode-locking technique removes that problem by moving this lossy semiconductor saturable absorber into the low-Q coupled cavity. This coupled cavity mode-locking technique, which uses a resonant nonlinearity inside the coupled cavity, is called resonant passive modelocking (RPM) and was first demonstrated with a Ti:sapphire laser [4], [5] and later with a Nd:YLF laser [6] using a p–i–n quantum-well reflector. However, a low-temperature MBE grown semiconductor absorber produces a larger nonlinearity which increases the overall mode-locking stability. In the case of a p–i–n quantum-well reflector, the nonlinearity is based on an ultrafast excitonic effect [7]. Therefore, the p–i–n quantum-well saturable absorber represents a fast saturable absorber which "instantly" responds to the incident pulse intensity envelope. In this case a theoretical mode can produce an analytical solution [5], [8]. This is not the case for the "semi-fast" LT semiconductor which will require more theoretical work. Both saturable absorbers, however, produced mode-locked pulse durations of a few picosecond.

Prior to RPM, an early example of coupled cavity mode locking is the soliton laser [9], which uses a fiber in the negative disperison regime, and therefore the soliton pulse shortening as the nonlinearity in the coupled cavity. Blow and Wood [10] discovered with their computer simulations that any nonlinear external cavity should produce mode locking. This prediction was followed by many passively mode-locked lasers using a normal dispersion fiber inside a coupled cavity, typically referred to as additive pulse mode locking (APM) [11]–[22]. Both soliton lasers and APM lasers are based on a reactive nonlinearity inside the coupled cavity, which requires a feedback system to control the cavity length for stable mode locking. In contrast, RPM is self-stabilized by optical frequency adjustments. This will be explained in more detail in Section II.

More recently, saturable-absorber-like mode locking was produced with an intracavity reactive nonlinearity, such as self-focusing [23]–[32] or nonlinear polarization

Manuscript received August 19, 1991; revised February 15, 1992.
The authors are with AT&T Bell Laboratories, Holmdel, NJ 07733.
IEEE Log Number 9200576.

rotation [33], [34] in the laser gain material. However, because the modelocking nonlinearity is based on an intracavity Kerr effect, these mode-locking techniques are not self-starting and need another starting mechanism. We have demonstrated that RPM with a very weakly coupled cavity can start self-focusing mode locking, resulting in stable 70 fs pulses using a Ti:sapphire laser [24]. Self-starting is a fundamental problem, because the Kerr effect is directly proportional to the peak intensity, which is very weak for noise spikes in CW lasers. In contrast, RPM is self-starting because the mode-locking nonlinearity, absorption bleaching of a semiconductor reflector, scales with the pulse energy.

Resonant passive modelocking has several key features for generating short pulses with a compact and reliable laser, such as: RPM is self-starting and does not require active cavity length control, one nonlinear semiconductor reflector works for any repetition rate, is a bulk device requiring no critical alignment, and is a compact nonlinearity (≈ 400 μm thick). A passively mode-locked diode-pumped solid-state laser such as RPM Nd:YLF offers a practical compact pulsed laser source with potentially several watts of average power at around 1.06 and 1.3 μm wavelength. The upper limit of the pulse repetition rate is ultimately given by the carrier lifetime in the quantum-well reflector which is in the picosecond and subpicosecond regime for low-temperature grown semiconductors [35].

In this paper, we present improved results using a low-temperature grown InGaAs–GaAs quantum-well reflector, which produced stable pulses as short as 3.7 ps [36]. Average output power has been as high as 550 mW at 250 MHz repetition rate with a pump power of 1.3 W from a CW Ti:sapphire laser. The low-temperature grown strained-layer InGaAs–GaAs multiple quantum-well device has several advantages: no surface striations, a larger nonlinearity, and a short carrier lifetime. The good stability and reproducibility has allowed a more detailed study of this mode-locking technique for Nd:YLF lasers.

II. Theoretical Background

A full theoretical model is given by Haus *et al.* [5] assuming an ideal fast saturable absorber. Here we review the RPM operation based on the intensity dependent coupled cavity reflectivity which provides a basic understanding of RPM. The coupled cavity setup for RPM is shown in Fig. 1 for both the standard (a) and the Michelson (b) coupled cavity configuration. We achieved good performance for both setups; however, for most reported results we used the standard configuration because of its simplicity [Fig. 1(a)].

The coherent superposition of the pulse in the main cavity with the pulse from the nonlinear coupled cavity can be described by modeling the laser coupling mirror and the external cavity as a nonlinear intensity dependent mirror. The reflectivity of this mirror R_{nl} is then referred to as the nonlinear coupled-cavity reflectivity. The amplitude coupled-cavity reflectivity r_{nl} is given by [5], [37] (assuming $r_1 > 0$, $r_2 > 0$, and $t > 0$)

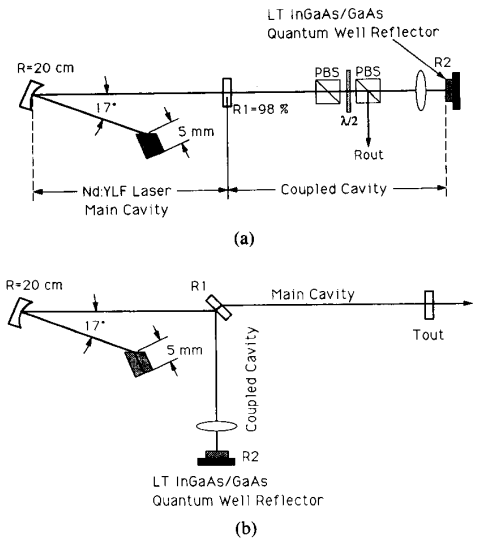

Fig. 1. RPM cavity design. (a) Standard and (b) Michelson type.

$$r_{nl} = \frac{-r_1 + t^2 r_2 e^{-2i\beta L'}}{1 - r_1 r_2 t^2 e^{-2i\beta L'}} \tag{1}$$

where, considering Fig. 1(a), $r_1^2 = R_1$ is the intensity reflectivity of the coupling mirror, $R_{out} = 1 - t^2$ is the intensity reflectivity of the output coupler, $r_2^2 = R_2$ is the intensity reflectivity of the semiconductor reflector, L' is the coupled cavity length, and β is the propagation constant. The intensity coupled cavity reflectivity R_{nl} follows from (1)

$$R_{nl} = r_{nl} r_{nl}^* = \frac{(r_1 - t^2 r_2)^2 + 4 r_1 r_2 t^2 \sin^2(\beta L')}{(1 - r_1 r_2 t^2)^2 + 4 r_1 r_2 t^2 \sin^2(\beta L')}. \tag{2}$$

The coupled cavity introduces a phase shift ϕ_{nl} defined by

$$R_{nl} = |R_{nl}| e^{-i\phi_{nl}} \tag{3}$$

which modifies the axial mode equation of the main cavity to

$$2\beta L + \phi_{nl} = 2\pi m \tag{4}$$

derived from the steady-state condition

$$e^{-2i\beta L} e^{-i\phi_{nl}} = 1 \tag{5}$$

where m is an integer, and L is the main cavity length. The axial mode equation (4) shows that the axial modes are slightly shifted due to the coupled cavity. The maximum coupled cavity intensity reflectivity R_{max} is at

$$\beta_{max} L' = (2m' - 1)\frac{\pi}{2} \tag{6}$$

where m' is an integer number. With (2) and (6), R_{max} is given by

$$R_{max} = \frac{(r_1 - t^2 r_2)^2 + 4 r_1 r_2 t^2}{(1 - r_1 r_2 t^2)^2 + 4 r_1 r_2 t^2}. \tag{7}$$

In addition, at maximum reflectivity $\phi_{nl} = 0$ which simplifies the axial mode equation (4) to

$$2\beta_{\max} L = 2\pi m. \tag{8}$$

From (2) alone follows that the periodicity of the coupled-cavity reflectivity R_{nl} is $c/2L'$. However, with the additional condition that the frequency has to be an axial mode of the coupled cavity (4), the coupled-cavity reflectivity has a periodicity of $c/2\delta L$, where δL is the cavity length detuning defined by $L' = L + \delta L$. This follows directly from the condition that $\beta_{\max}$ has to fulfill both (6) (being at maximum coupled cavity reflectivity) and (8) (being an axial mode of the coupled cavity). Therefore, the wave vector period $\Delta\beta$ is given by

$$2\,\Delta\beta\,\delta L = 2\pi \tag{9}$$

The frequency period Δv and wavelength period $\Delta\lambda$ is then given by

$$\Delta v = \frac{c}{2\,\delta L} \quad \text{and} \quad \Delta\lambda = \frac{\lambda^2}{2\,\delta L}. \tag{10}$$

Fig. 2 shows the coupled cavity reflectivity for both an amplitude [Fig. 2(a)] and a phase nonlinearity [Fig. 2(b)]. In the case of an amplitude nonlinearity, R_2 is intensity dependent, and we achieve an intensity dependent reflectivity at the maxima of the coupled cavity reflectivity $R_{\max}$ (7). $R_{\max}$ is higher at higher intensities and lower at lower intensities, which therefore, reduces the gain in the low-intensity wings of the pulse and narrows the pulse each cavity round-trip [Fig. 2(a)].

In the case of a phase nonlinearity, the intensity dependent phase shift can be treated as an intensity dependent cavity length detuning $\delta L(I)$, which shifts the frequency for maximum reflectivity (6). Assuming that the laser is self-adjusting its center frequency to maximum reflectivity, no intensity dependent reflectivity is introduced by the nonlinear phase shift. Therefore, in order to obtain an intensity-dependent reflectivity the laser must be held at a center frequency v_0 that does not correspond to maximum gain [Fig. 2(b)]. An APM laser is operated at this center frequency. From Fig. 2(b) it becomes clear that on only one slope is the reflectivity higher at higher intensity and lower at lower intensity. Therefore, interferometric absolute cavity length stabilization is required. This explains why the APM laser has a tendency to drop out of mode-locked operation induced by sudden mechanical vibrations that cannot be tracked by a simple feedback circuit.

Any cavity length fluctuation will change $\beta_{\max}$ (6). Thus, without an active cavity length control, the center wavelength adjusts itself for maximum coupled-cavity reflectivity which corresponds to maximum gain. This self-adjustment of the optical frequency maintains a coherent superposition of the pulses at the coupling mirror and, therefore, stable mode locking. We have experimentally demonstrated this self-stabilization with an RPM Ti : sapphire laser by actively changing the coupled-cavity length with a piezo-transducer and monitoring the optical spectrum shifting its center wavelength accordingly without affecting the stable mode-locked pulse train [4]. This self-stabilization by optical frequency adjustments is a basic property of two coupled linear cavities.

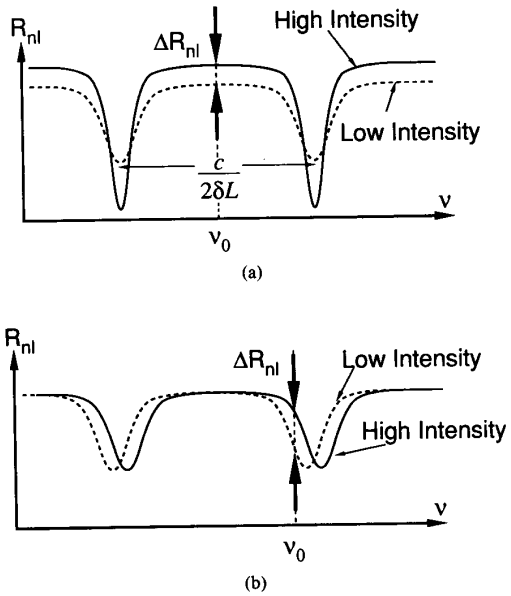

Fig. 2. Coupled cavity reflectivity. (a) Amplitude nonlinearity (RPM) and (b) phase nonlinearity (APM).

It is interesting to realize, that due to the self-frequency adjustments to maximum coupled cavity reflectivity, the nonlinear phase shift associated with the nonlinear absorption change in the quantum-well reflector (determined by the Kramers–Kronig relations) has no effect on RPM. However, even without the self-frequency adjustments the nonlinear phase shift has negligible effect on RPM as long as the nonlinear phase shift is much smaller than π.

The coupled cavity acts as a small perturbation on the main high-Q laser cavity. For stable and self-starting mode locking, R_1 [in Fig. 1(a)] was typically large ($\approx 98\%$). Therefore, similarly to the theoretical treatment of the APM laser [38], the intensity dependent coupled cavity reflectivity can be approximated by

$$R_{nl} = R_{\max} + \left(\frac{\partial R_{\max}}{\partial R_2}\right) \Delta R_2(E_p) \tag{11}$$

where E_p is the pulse energy density incident onto the quantum-well reflector, and the factor $\Delta R_2(E_p)$ is the nonlinear reflectivity change due to absorption bleaching in the semiconductor reflector. In the short pulse limit (pulsewidth $\tau <$ carrier lifetime) and at a pulse repetition period larger than the carrier lifetime, ΔR_2 is determined by the pulse energy density E_p and is, therefore, independent of τ. The nonlinear reflectivity can be custom designed by using different focusing lenses (which changes the pulse energy density), different absorber thicknesses, and slightly different position of the bandgap energies.

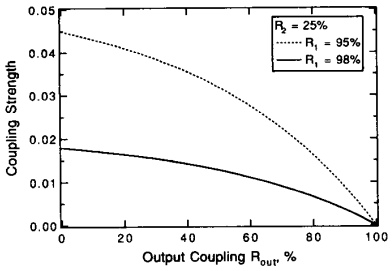

Fig. 3. Calculated coupling strength $\partial R_{max}/\partial R_2$.

However, especially, for the low-temperature MBE grown InGaAs–GaAs quantum-well reflectors these design parameters are not yet fully understood and will require further work. The factor $(\partial R_{max}/\partial R_2)$ is determined by the laser cavity parameters [see (7)] and defines the coupling strength between the two cavities for a given amplitude nonlinearity ΔR_2. The coupling strength $\partial R_{max}/\partial R_2$ is shown in Fig. 3 for typical cavity parameters.

III. Experimental Setup and Results

The experimental setup is shown schematically in Fig. 1. The main cavity is an end-pumped astigmatically compensated standing-wave folded cavity. A 5 mm Nd:YLF rod has its flat end coated for high-reflection at the lasing wavelength (1.047 μm) and antireflection coated for the pump wavelength with the other end cut at Brewster's angle. This cavity is described in more detail in [6]. An AR coated, slightly wedged laser rod prevents stable mode locking due to residual reflections from the AR coated side, which interferes with the low-intensity pulse reinjected from the coupled cavity.

The amplitude nonlinearity is based on absorption bleaching of a low-temperature ($\approx$380°C) MBE grown InGaAs–GaAs multiple quantum-well structure with 50 periods of 60 Å thick GaAs barriers and 62 Å $In_xGa_{1-x}As$ wells with $x = 0.29$ [Fig. 4(a)]. The LT MQW structure is grown on top of a AlAs–GaAs dielectric mirror stack with 10 periods of 905 Å AlAs and 764 Å GaAs layers grown at normal ($\approx$640°C) temperature on a GaAs substrate. A mirror stack grown on a GaAs substrate underneath the saturable absorber layer provides a good sink and makes any residual étalon effects negligible due to a large free spectral range of $\approx$160 nm. The bandgap of the MQW absorber layer is close to the lasing wavelength of 1.047 μm. We typically used a 5× or 10× lens to focus the laser beam onto the LT InGaAs–GaAs quantum-well reflector with peak intensities as high as $\approx$50 MW cm^{-2} (average intensity $\approx$60 kW cm^{-2}) producing a high carrier concentration which bleaches the absorption and increases the reflection of the quantum-well reflector.

Low-temperature grown InGaAs–GaAs MQW layers provide an optically smooth surface [39], and the carrier lifetime is reduced to the picosecond regime (see pump probe experiment in Section IV). Due to the lattice mismatch of InGaAs on GaAs, the InGaAs–GaAs MQW layer is strained and if grown at normal temperature (500°C) exhibits surface striations which degraded the performance of the RPM Nd:YLF laser [6], [40]. Low temperature grown materials exhibit significant unsaturable losses. However, the mode-locking process is not very sensitive to these unsaturable losses because the main laser is the high-Q cavity, whereas the coupled cavity is a low-Q cavity from which as much as 85% of the light is coupled out.

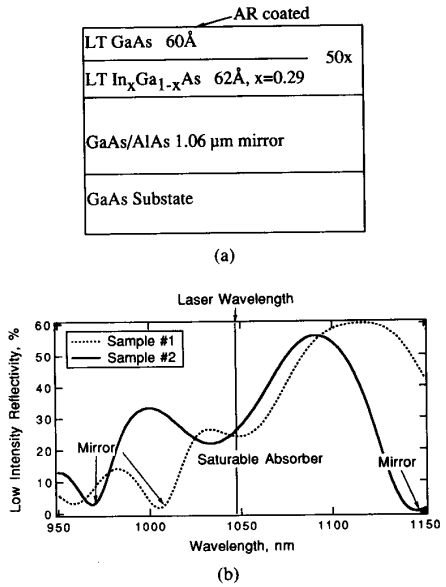

Fig. 4. (a) LT InGaAs–GaAs quantum-well reflector. (b) Low intensity reflectivity for sample #1 and #2.

Fig. 4(b) shows the measured low-intensity reflectivity of two samples with slightly different band-gap energies close to the lasing wavelength. These samples are from different positions of the wafer which was not rotated during the MBE growth. The dielectric mirror had $\approx$120 nm width [Fig. 4(b)]. Both samples modelocked the Nd:YLF laser. They only differ in the required pulse energy to bleach the absorption which will be discussed below. The sample was initially mounted on a thermoelectric cooler. However, the modelocking performance was not significantly affected by a temperature change from 10°C to 50°C because the position of the band-gap energy is not very critical [see Fig. 4(b)]. We later removed the thermoelectric cooler and simply indium-soldered the sample on a copper heat sink.

We generated pulses as short as 3.7 ps (Fig. 5) without an active cavity length control. An ideal 3.7 ps sech^2 pulse shape is fitted to the autocorrelation trace (dashed curve in Fig. 5). The Nd:YLF laser in the Michelson configuration [Fig. 1(b)] was CW pumped with 1.6 W at the 797 nm wavelength of a Ti:sapphire laser. With a 2% output coupler T_{out} the average output power was 330 mW at $\approx$250 MHz. The tunable coupling mirror R_1 simply consisted of a 0.375″ thick fused quartz substrate (not AR

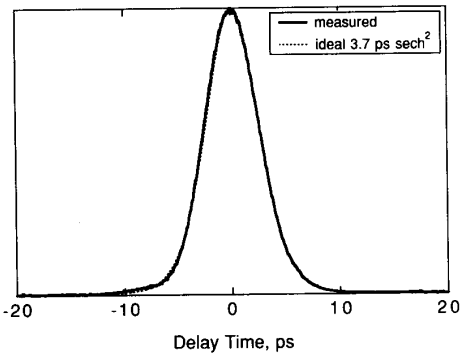

Fig. 5. Real-time noncollinear autocorrelation trace; experimental result (solid curve), and an ideal 3.7 ps sech^2 pulse (dashed curve).

coated on either side) on a goniometer using the angle of incidence as a reflectivity tuning element and was set for $R_1 \approx 0.8\%$ reflectivity. The cavity length detuning was approximately -0.4 mm.

We achieve similar results with the standard cavity configuration [Fig. 1(a)] using a 2% coupling mirror [$R_1 = 98\%$ in Fig. 1(a)]. The slope efficiency of the main laser is 49% and the pump threshold is at 23 mW. A tunable output coupler R_{out} inside the coupled cavity is formed with a half-wave plate and two polarizing beam splitters. We typically achieved self-stabilized pulses with a pulsewidth ≈ 4.5 ps and a repetition rate of 250 MHz at cavity length detunings ≈ -0.4 mm. The pulse width is decreasing with decreased cavity length detuning; however, self-stabilization does not work at close to matched cavity length ($\delta L < 0.4$ mm) which will be discussed in more detail in Section IV. With a 10× focusing lens, Sample #2 [Fig. 4(b)] and a pump power of 1.3 W, the average output power was 550 mW with R_{out} [Fig. 1(a)] as high as 85%. Sample #1 [Fig. 4(b)], with its bandgap at longer wavelength, required a slightly higher bleaching energy and the average output power was 510 mW with R_{out} as high as 79%. In both cases the mode-locking process was self-starting and controlled by the coupled cavity. Using sample #2, the RPM Nd:YLF laser was stable and self-starting for pump power as low as 0.4 W thereby reducing R_{out} to 70%.

The mode locking is self-starting and controlled by the quantum-well reflector. As soon as we block the coupled cavity the laser immediately falls back into cw operation and when unblocked the laser immediately starts to mode lock. There is a limited range for R_{out} at which the laser is stably mode locked (without self-Q-switching) and self-starting. By decreasing R_{out} too much, thereby increasing the coupling strength (11), the laser starts to self-Q-switch (see further discussion in Section IV).

Using an output coupler R_{out} as high as 85% makes the coupled cavity a very low-Q cavity. In addition, the Q is further reduced by the low reflectivity of the quantum-well reflector. Therefore, it is important to realize that inside the coupled cavity the beam coming directly from the main cavity is much stronger than the reflected beam, and this stronger beam is used as the main output. The first polarizing beamsplitter is used to measure the reflected intensity and to prevent any feedback into the laser at a different polarization.

IV. Discussions

A. Time-Resolved Nonlinear Reflectivity of Quantum-Well Saturable Absorber

Using the RPM Nd:YLF laser described above (standard cavity configuration and with sample #2) we performed a standard noncollinear pump-probe experiment to determine the nonlinear reflectivity change and the carrier lifetime of sample #1. The pump-probe experiment is shown schematically in Fig. 6(a) where we use a slow-scan translation stage as the variable time delay of the probe pulse. We used for both beams a 10× focusing lens. The probe beam intensity was sufficiently low so that no reflectivity changes were introduced by the probe. Fig. 6(b) shows the time-dependent nonlinear reflectivity of sample #1 at different excitation energy densities comparable to the ones used in the RPM laser. Superimposed is the measured autocorrelation pulse of the 5.3 ps pulses from the RPM Nd:YLF laser used to perform this measurement.

The nonlinear reflectivity change is due to absorption bleaching of the quantum-well reflector. The exponential decay time corresponds to a 25 ps carrier lifetime and is as expected constant for all excitation densities. The maximum reflectivity change ΔR_2 shows still no saturation effects, and increases linearly with increased pulse energy. For an excitation energy density of ≈ 0.8 mJ cm^{-2}, we measured a 6% reflectivity change. Given a ΔR_2 of 6%, and a coupling strength $\partial R_{max}/\partial R_2$ of 0.005 (Fig. 3, $R_1 = 98\%$, $R_2 = 25\%$, and $R_{out} = 85\%$), the nonlinear coupled cavity reflectivity change is only 0.03% (11). This is, however, sufficient to mode lock the laser.

B. Dependence on Focusing Lens

As mentioned before one of the design parameters for the quantum-well reflector is the focusing length which can be optimized for maximum output power (i.e., maximum R_{out} in Fig. 1). For sample #2, Fig. 7 displays the maximum R_{out}, as a function of focusing length and focused laser beam diameter, for which the RPM Nd:YLF laser is still stably mode locked and self-starting. In all cases, the mode-locked pulsewidth is 5 ps and the Ti:sapphire pump power is 1.3 W. Fig. 7 shows that the onset of mode locking is determined by the pulse energy density on the saturable absorber reflector, which determines the strength of the nonlinearity. The required pulse energy density and, therefore, the required ΔR_2 [Fig. 6(b)] decreases with reduced R_{out} because the coupling strength becomes larger [Fig. 3 and (11)].

C. Dependence on Cavity Length Detuning

Fig. 8 shows the measured autocorrelation, optical spectrum and sampling scope pulse of the RPM Nd:YLF

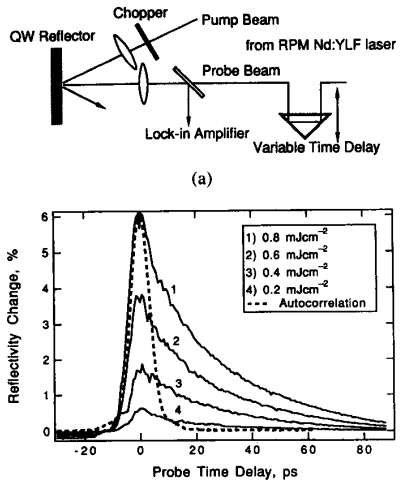

Fig. 6. (a) Noncollinear pump-probe setup. (b) Time resolved reflectivity of the quantum well reflector for different excitation energy densities. Superimposed is the autocorrelation trace of a 5.3 ps pulse from the RPM Nd:YLF. Device under test is sample #1, sample #2 is used to mode lock the Nd:YLF laser.

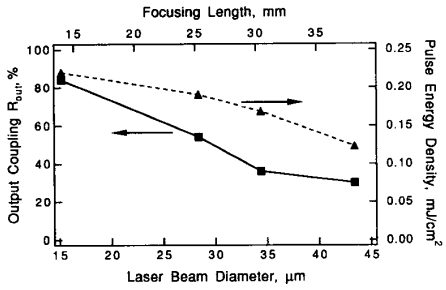

Fig. 7. Focusing lens as a saturable absorber design parameter.

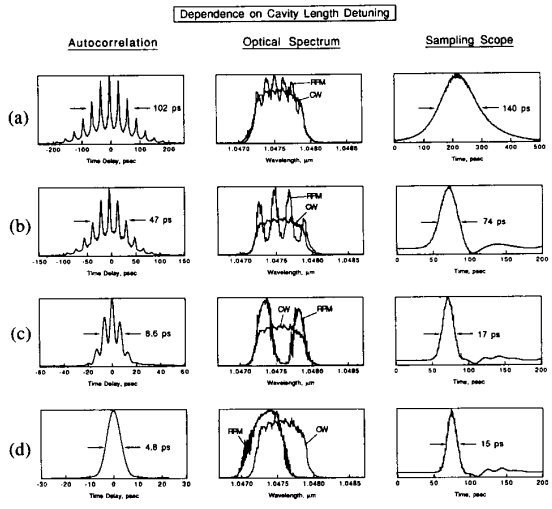

Fig. 8. Dependence on cavity length detuning for autocorrelation, optical spectrum and sampling scope trace. Cavity length detuning (a) 4.6 mm, (b) 2.6 mm, (c) 0.9 mm, and (d) 0.33 ± 0.22 mm.

laser as a function of cavity length detuning. We used the standard cavity configuration [Fig. 1(a)], a pump power of 1.3 W, a coupling mirror transmission $1 - R_1$ of 2%, and an output coupler R_{out} between 50 and 85%, with lower output coupling at larger cavity length detuning (i.e., at $\delta L = -0.5$ mm, $R_{out} = 85\%$, and at $\delta L = -3$ mm, $R_{out} = 60\%$). At $\delta L = -3$ mm the pulse duration is larger than the carrier lifetime in the saturable absorber which reduces the nonlinear reflectivity ΔR_2. Therefore, for stable mode locking the coupling strength has to be increased by reducing R_{out} (Fig. 3). The focusing lens for the quantum-well reflector was a long-working-distance 10× lens. The overall output power was 550 mW with $R_{out} = 85\%$. The mode locking at all positions is self-starting and controlled by the quantum-well reflector; when the coupled cavity was blocked, the laser immediately falls back into CW operation, and when unblocked, the laser immediately started to mode lock. Qualitatively the same results as shown in Fig. 8 were observed with a 5% coupling mirror and the Michelson cavity configuration [Fig. 1(b)].

We used a real-time noncollinear autocorrelation. But for longer pulses (>60 ps), a slow scan system was used. The optical spectrum was measured with an optical spectrum analyzer with 0.1 nm resolution. We used a high speed InGaAs photo detector with a ≈50 GHz bandwidth and a 50 GHz sampling head. All instruments were computer interfaced.

Both the autocorrelation traces and the sampling scope pulse in Fig. 8 and Fig. 9(a) show that the pulsewidth continuously increases with increased cavity length detuning, similarly to the RPM Ti:sapphire [4], [5]. The pulse broadening at larger δL is easily explained in the time domain: the total steady-state pulse is a coherent superposition of the pulse in the main cavity and the slightly delayed or advanced reinjected pulses from the coupled cavity. Therefore, at larger cavity length detuning the resulting pulse duration increases. In contrast to the smooth autocorrelation traces of the RPM Ti:sapphire laser [4], [5] the autocorrelation traces of the Nd:YLF laser exhibit a picosecond spike structure on top of a longer pulse, with the spikes equally spaced by the cavity detuning time $t_{pp} = 2\,\delta L/c$ [Fig. 9(a)], where c is the velocity of light and δL is the cavity length detuning.

The pulses acquire more excess bandwidth at larger cavity length detuning δL, as predicted by Haus's theory [5]. The measured excess bandwidth [Fig. 9(c)] is defined by the ratio of the FWHM optical spectrum [Fig. 9(b)] to the time-bandwidth limited spectral width of the pulse envelope, assuming a sech^2 pulse shape [Fig. 9(a)]. The measured excess bandwidth for $\delta L < 0.7$ mm (no subspectral lines) is an upper limit because it is a time-averaged optical spectrum and includes the self-frequency shifts which compensate for any cavity length fluctuations. Additionally, at larger cavity length detuning the optical spectrum shows a subspectral structure (Fig. 8) with a period given by $\lambda^2/2\,\delta L$ introduced by the wavelength dependence of the coupled cavity reflectivity [(10)

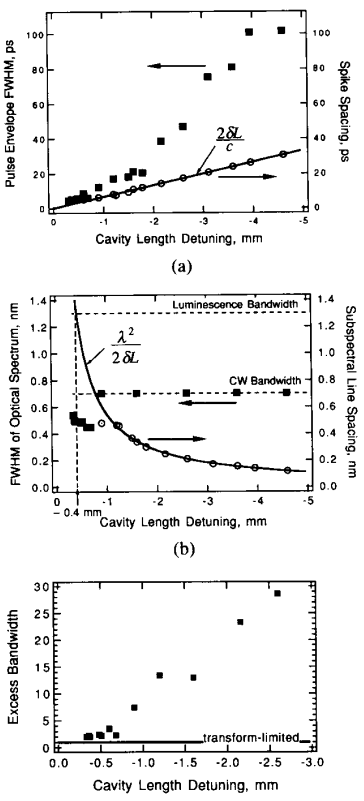

Fig. 9. (a) Pulsewidth and spike separation on autocorrelation, (b) optical spectrum, and (c) excess bandwidth as a function of cavity length detuning.

and Fig. 9(b)] and with a FWHM equal to the CW spectrum [Fig. 8 and 9(b)]. Only at smaller cavity length detuning, when the coupled cavity reflectivity period (9) is compared to the CW spectrum we observe one spectral line with a FWHM smaller than the CW spectrum [Fig. 8(d) and 9(b)].

The difference in the optical spectrum of the RPM Nd:YLF compared to the RPM Ti:sapphire laser is due to the much higher gain in the Nd:YLF laser. The small signal gain of the Nd:YLF laser was more than 100%, whereas of the Ti:sapphire laser was only $\approx 15\%$. Therefore, as shown in Fig. 8, the Nd:YLF laser is lasing at the full CW spectrum, but modified by the wavelength dependence of the coupled cavity reflectivity [(10) and Fig. 2(a)], whereas the RPM Ti:sapphire laser is lasing with a time-averaged optical spectral width approximately equal to the periodicity of the coupled cavity reflectivity [4], [5]. Thus, at larger cavity length detuning ($\delta L >$ 0.5 mm), the RPM Nd:YLF laser has a larger excess bandwidth, which enhances the coherence spike structure on the autocorrelation trace.

D. Coherence Spikes or Multiple Pulsing?

We have shown that the pulses have excess bandwidth at larger cavity length detuning [Fig. 9(c)], therefore, coherence spikes [41], [42] are expected. With RPM the steady-state pulse is a coherent superposition of the pulse in the main cavity and many delayed or advanced pulses from the coupled cavity. Consider a nontransform limited pulse and assume the pulse spectrum is heterodyned n times with each spectrum shifted by $\Delta\nu$, where $1/\Delta\nu$ is the cavity length detuning time $2\ \delta L/c$. Because all spectra are coherent, they produce a coherence spike at zero time delay and at each time delay where the carrier phases coincide. The result is an autocorrelation function with $2n + 1$ coherence spikes with a 2:1 peak-to-background ratio (assuming noncollinear autocorrelation), spaced by $2\ \delta L/c$, and a FWHM spike width inversely proportional to the spectral width of the pulse. This is consistent with our observation (Figs. 8 and 9). However, close to the maximum cavity length detuning, where the laser is still modelocked, the laser clearly breaks up into multiple pulsing [Fig. 8(a)].

Even though the Nd:YLF laser is homogeneously broadened, spatial hole burning introduces inhomogeneous broadening. Because the FWHM of the picosecond spikes are only determined by the overall spectral width and are independent of the subspectral linewidth [Fig. 10(a)], the subspectral lines must be phase locked to each other due to the saturable absorber. However, the argument that the subspectral lines are correlated to different pulses, each with its own carrier frequency, is not supported experimentally: n pulses would give $2n - 1$ autocorrelation pulses which is in contradiction to our experimental results [Fig. 8(b) and (c)].

The transition from coherence spikes to multiple pulsing must happen gradually. For example, at relative large cavity length detunings we discovered that there is still some multiple pulsing contribution even though the autocorrelation shows a 2:1 intensity ratio and approximately the theoretically predicted FWHM of the spikes given by $4\sqrt{2}/\Delta\omega = 4.7$ ps with $\Delta\lambda = 0.7$ mm [41], [42].

Therefore, Fig. 10(a) indicates that the autocorrelation spikes are coherence spikes. However, the existence of multiple pulsing is shown with a 50 GHz photodetector and a 40 GHz microwave spectrum analyzer which are insensitive to coherence effects. Fig. 10(b) clearly shows a second laser harmonic peak at 38 GHz ($= c/2\ \delta L$, with $\delta L = 4$ mm) which is expected when the picosecond spikes are not due to coherence effects alone. The energy contained in the short multiple pulses is much smaller than the energy contained in the longer background pulse. Thus we were unable to detect multiple pulsing features with the photodetector and high-speed sampling scope (Fig. 8).

We used the pump-probe experiment described above to prove that at cavity length detunings of less than 2 mm, the multiple spike structure on the autocorrelation trace is only a coherence effect. Fig. 11 shows the measured reflectivity change for parallel (a) and perpendicular (b) polarization of the pump and probe beam. The measurement with parallel polarization exhibits coherence effects due to four-wave mixing, whereas with perpendicular polar-

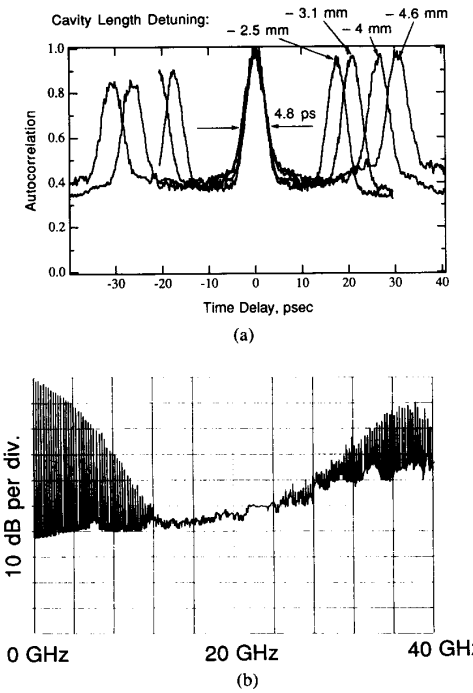

Fig. 10. *Multiple pulsing regime* ($|\delta L| > 2$ mm): (a) Zoomed-in autocorrelation traces at different cavity length detunings δL and (b) RPM pulse monitored with a microwave spectrum analyzer at $\delta L = -4$ mm.

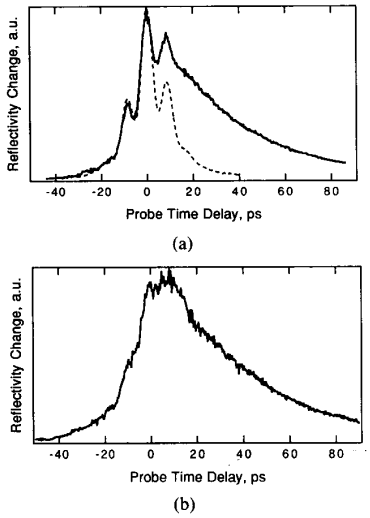

Fig. 11. *Coherence spike regime* (0.8 mm < $|\delta L|$ < 2 mm): Pump-probe experiment on sample #2 using the RPM Nd:YLF laser with $\delta L = -1.2$ mm using (a) parallel and (b) perpendicular polarization of pump and probe pulse. Superimposed in (a) is the autocorrelation (dashed curve).

ization no coherence effects exist. If there were multiple pulses present, we would observe them in both cases. However, Fig. 11 clearly demonstrates that the spike structure on the autocorrelation trace [dashed trace in Fig. 11(a)] is a coherence effect. The pulse used in this experiment was generated by the RPM Nd:YLF laser at a cavity length detuning of -1.3 mm. Using this technique, we started to observe multiple pulsing effects for $|\delta L|$ larger than 2 mm.

E. Limits for Self-Stabilization and Magnitude of Frequency Fluctuations

As discussed in more detail in Section II, the RPM laser is self-stabilized by small frequency shifts. The laser corrects for any relative cavity length fluctuations by an adjustment of the center wavelength for maximum coupled cavity reflectivity (6). This wavelength adjustment maintains coherent superposition at the coupling mirror. The laser is self-stabilized as long as the gain bandwidth of the Nd:YLF laser can support the required self-wavelength shifts.

The maximum wavelength shift, required to compensate for any cavity length fluctuations in a freely running RPM laser, is determined by the coupled cavity reflectivity period $\lambda^2/2\ \delta L$ shown in Fig. 9(b) (10). Thus, this wavelength fluctuations become smaller at larger cavity length detuning. RPM does not require absolute cavity length control, because drifts of several 100 μm are required for significant pulse width changes [Fig. 9(a)]. At small cavity length detunings, the self-wavelength shifts can go beyond the CW bandwidth because the periodic reflectivity modulation effectively reduces the gain in the center and increases the gain in the wings of the gain bandwidth [43]. Fig. 8(d) demonstrates such a case where the modelocked spectrum reaches beyond the CW bandwidth. The upper limit of wavelength shifts still supported by the laser is determined by the 12 cm^{-1} fluorescence bandwidth of Nd:YLF [44], corresponding to a 1.3 nm bandwidth. Therefore, consistent to our experimental results the minimal cavity length detuning for self-stabilization is around 0.4 mm at which the coupled cavity reflectivity period (10) is equal to the fluorescence bandwidth [Fig. 9(b)].

F. AM Noise and Self-Q Switching

The stability is much better for negative cavity length detunings (i.e., $\delta L < 0$) where the reinjected pulse is ahead of the pulse in the main cavity. The peak-to-peak amplitude fluctuations are 2.5% measured with an oscilloscope over a 100 ms span using a >10 MHz detection bandwidth. The high-frequency AM noise, characterized with a photo detector and a microwave spectrum analyzer, is limited by the Ti:sapphire (more precisely the argon ion) pump laser, similar to a passively mode-locked CPM laser [45].

Fig. 12(a)–(c) determines the noise sidebands of the RPM Nd:YLF laser at a cavity length detuning ≈ -0.4 mm for different frequency spans with 10 dB per division in the vertical axis. With a shot noise level of -154.9 dBc in 1 Hz bandwidth at 1 mA of photocurrent, the AM noise in numbers of dB above the shot noise is then summarized in Fig. 12(d). With Fig. 12(d), the minimum de-

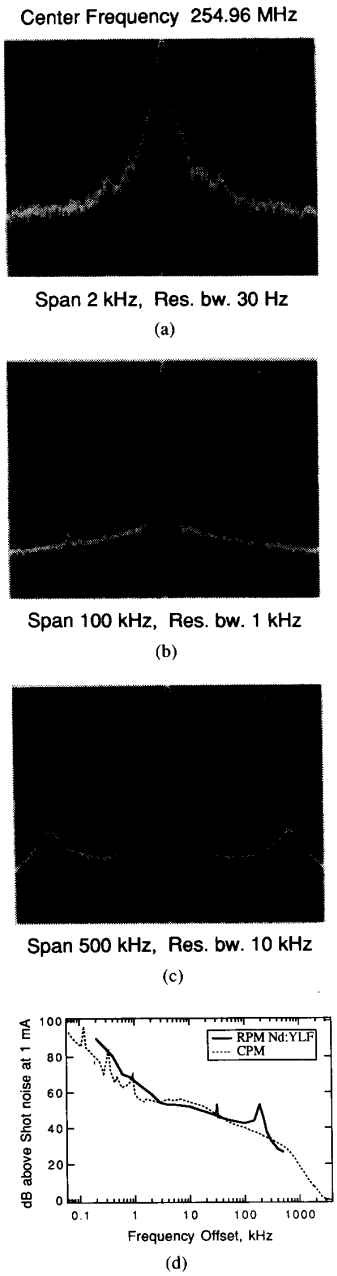

Fig. 12. AM noise sidebands around the first laser harmonic with 10 dB per division at (a) 2 kHz frequency span, (b) 100 kHz span, and (c) 500 kHz span. The relaxation oscillation peaks at ≈ 180 kHz frequency offset. (d) AM noise sidebands in dB above shot noise at 1 mA of photocurrent in comparison to a CPM Rhodamine 6G laser.

tectable signal for any experiment can be easily determined [46]. The noise spike at around ≈ 180 kHz [Fig. 12(c) and (d)] is due to the relaxation oscillation of the Nd:YLF laser. The strength of the relaxation frequency noise is typical for any CW mode-locked Nd:YLF laser. The AM noise at large frequency offsets (> a few 100 kHz) is limited by the argon-ion laser noise and can be reduced with diode-pumping.

The Nd:YLF laser has a tendency for self-Q-switching. A Nd:YLF laser self-Q-switches at the relaxation oscillation frequency, which strongly AM modulates the modelocked pulse train. Therefore, a microwave spectrum analyzer shows very strong modulation sidebands next to the mode-locked laser harmonic at the pulse repetition rate of ≈ 255 MHz [Fig. 13(a)]. The increased sidebands at the relaxation oscillations can be compared to Fig. 12(c) where the laser was modelocked but not self-Q-switched mode locked. An oscilloscope [Fig. 13(b)] shows that the mode-locked pulse train (not resolved) is strongly modulated and the pulse train envelope has a period determined by the relaxation oscillation frequency of ≈ 170 kHz (note that the exact relaxation oscillation frequency depends on the pump power). Note that we observed stable autocorrelation traces and stable sampling scope traces even when the laser was self-Q-switched.

The tendency for self-Q-switching is higher at higher coupling strength [(11) and Fig. 3] and a large nonlinear reflectivity which increases the nonlinearity. This is consistent with the discussion given by Haus [47]. In addition, the tendency for self-Q-switching is enhanced in the presence of higher order transverse modes which increase amplitude fluctuations and relaxation oscillations of the Nd:YLF laser. With an intracavity aperture, we can completely suppress higher order transverse modes. Because of the large dynamic range of the microwave spectrum analyzer (i.e., 30 dBm to -140 dBm) and the nondegeneracy of the higher transverse modes from the axial modes for our cavity design, we are able to maintain clean TEM_{00} mode of operation with extremely high sensitivity. Fig. 14 shows the microwave spectrum analyzer display over 1 GHz frequency span with (a) and without (b) higher transverse modes. The pulse repetition rate is 255 MHz and the roll-off of the laser harmonics is due to the limited bandwidth of the photo detector. The higher transverse modes are suppressed by slightly reducing an intracavity aperture size, thereby reducing the output power by $\approx 5\%$. Even though we use sometimes an intracavity aperture, self-focusing does not significantly contribute to the mode-locking process. We achieve mode locking without the intracavity aperture and the Nd:YLF laser drops into CW operation as soon as we block the coupled cavity (compare discussion in [24] and [32]).

G. Active Cavity Length Control?

As discussed above, the RPM laser self-stabilizes at the expense of small optical frequency shifts of maximum $c/2\ \delta L$, where δL is the cavity length detuning. Figs. 8 and 9 demonstrate that shorter pulses with less excess bandwidth are achieved at smaller cavity length detuning. Therefore, an active cavity length control can provide even shorter pulses at close to matched cavity length ($\delta L < 0.4$ mm) where the laser is not self-stabilized any more. In addition, an active cavity length control can eliminate

(a)

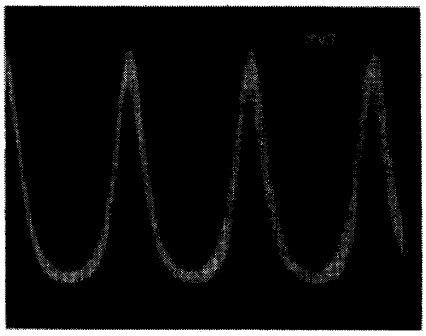

(b)

Fig. 13. Self-Q switching (a) microwave spectrum analyzer display with 10 dB/div at 500 kHz span, and (b) pulse train envelope on an oscilloscope.

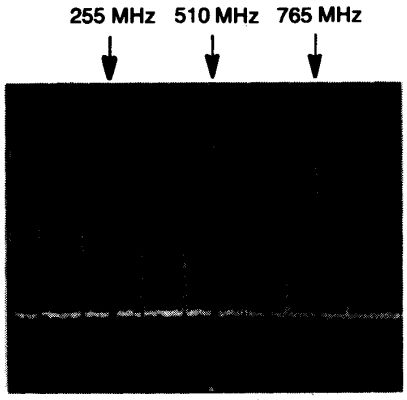

(a)

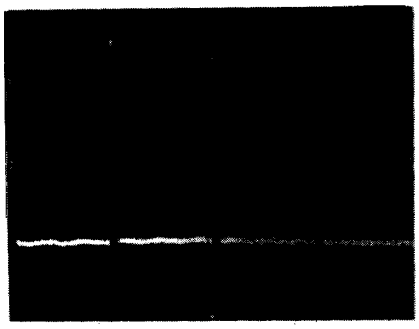

(b)

Fig. 14. Pulses monitored on a microwave spectrum analyzer (a) with higher order transverse modes and (b) without.

the small optical frequency fluctuations. We have constructed a very simple electronic feedback loop which corrects the coupled cavity length with a piezo-transducer. The error signal is based on the wavelength shifts of the optical spectrum measured with a photodetector after a grating and a knife edge. Generally, an active cavity length control circuit for an RPM laser is much simpler than for APM because no absolute interferometric cavity length stabilization is required.

V. Conclusion

We have demonstrated stable nearly transform-limited ≈ 4 ps pulses from an RPM Nd:YLF laser using a LT InGaAs–GaAs quantum-well reflector in a low-Q coupled cavity. As much as 85% of the power is coupled out of the external cavity, and 2% from the main laser. The laser is self-starting, self-stabilized, and controlled by the quantum-well reflector. As soon as we block the coupled cavity the laser immediately falls back into cw operation and when unblocked the laser immediately starts to mode lock. We fully characterized the AM noise of the laser.

The mode-locking mechanism is based on a fast reflectivity modulation from a quantum-well reflector in the coupled cavity. The nonlinearity is produced by absorption bleaching of a low-temperature MBE grown semiconductor reflector. The low-temperature growth generates the short carrier lifetime required for a "fast" saturable absorber. We have described the nonlinear coupled cavity as a nonlinear intensity dependent mirror. Based on this coupled cavity reflectivity we discussed the self-stabilization and the mode-locking process. More work is required to study the mode-locking regime using a "semi-fast" saturable absorber. We produced ≈ 4 ps pulsewidths with a ≈ 25 ps recovery time of the saturable absorber.

The pulse duration can be increased by simply increasing the coupled cavity length. The pulses, however, have more excess bandwidth at larger cavity length detunings (i.e., difference between main cavity length and coupled cavity length). This excess bandwidth is responsible for coherence spikes in the autocorrelation trace for coupled cavity detunings of more than 0.8 mm and less than 2 mm. At cavity length detunings of more than 2 mm the mode-locked pulse breaks up into several pulses superimposed on a longer background pulse. The smaller subpulses are separated by the cavity detuning time.

The laser is self-stabilized by optical frequency adjust-

ments. This means that small frequency shifts compensate for any relative cavity length fluctuations between the coupled cavities. These frequency shifts are the smaller the larger the cavity length detunings. The magnitude of the frequency fluctuations is given by $c/2\ \delta L$, where δL is the cavity length detuning. No self-stabilization can be obtained for δL smaller than 0.4 mm limited by the gain bandwidth of the laser.

The onset of mode locking is determined by both the pulse energy density, incident onto the quantum-well reflector, and the coupling strength between the two cavities. By reducing the focused beam size on the quantum-well reflector, we were able to increase the output coupler to as high as 85% and still achieve stable mode locking. The RPM Nd:YLF laser has also been used to measure the carrier lifetime. This measurement showed the nonlinearity is based on a "semi-fast" saturable absorber with a 25 ps carrier lifetime and a nonlinear reflectivity change of $\leq 6\%$. To further improve the saturable absorber performance, we are currently investigating different growth parameters, such as absorber thickness, growth temperature and the use of LT bulk materials.

Because of the long upper state lifetime the Nd:YLF laser has a tendency to self-Q-switch. However, we were able to completely control that mode of operation. We can switch from stable CW mode locking to stable self-Q-switched mode locking by simply increasing the coupling between the two cavities. In the self-Q-switched operation the mode-locked pulse train envelope is strongly modulated at the relaxation frequency (≈ 170 kHz) and produces stable picosecond (≈ 4 ps) pulses. A Q-switched mode-locked operation produces higher peak powers which give a higher conversion efficiency in nonlinear processes such as second harmonic generation. In addition, we believe that the self-Q-switching is strongly influenced by the "semi-fast" response time of the saturable absorber, which is currently under further investigations.

The low-temperature grown semiconductor reflector acts as a passive mode locker producing stable pulses at repetition rates ultimately limited by its carrier lifetime. At high repetition rates such a passive mode locking technique is especially advantageous because an expensive high-power (typically >1 W) microwave driving circuit typically used for active mode locking is not required. In addition, we have previously demonstrated that such a quantum-well reflector can be used as reliable starting mechanism for self-focusing mode-locking producing <100 fs pulses [24].

A diode-pumped RPM Nd:YLF laser is an all-solid state passively mode-locked laser source with a potential output power of watts, and which may find applications in optical computing as an external optical power supply, in optical testing of integrated circuits, in laser surgery and diagnostics, in displays, and in optical memories as a high-power quasi-CW green and blue laser source using the increased second harmonic conversion efficiency of the short pulses.

Acknowledgment

The authors wish to thank M. Zirngibl for helpful discussions about low-temperature grown InGaAs–GaAs materials and some samples for initial feasibility tests. Also G. D. Boyd for the 1.06 μm mirror design, H. A. Haus, and E. P. Ippen for helpful discussions, the Lightwave Electronics Corp. for the Nd:YLF crystal, and D. G. Coult for the AR coating of the quantum-well reflectors.

References

[1] P. W. Smith, Y. Silberberg, and D. A. B. Miller, "Modelocking of semiconductor diode lasers using saturable excitonic nonlinearities," *J. Opt. Soc. Amer. B*, vol. 2, pp. 1228–1229, 1985.

[2] M. N. Islam, E. R. Sunderman, C. E. Soccolich, I. Bar-Joseph, N. Sauer, T. Y. Chang, and B. I. Miller, "Color center lasers passively mode locked by quantum wells," *IEEE J. Quantum Electron.*, vol. 25, pp. 2454–2463, 1989.

[3] R. S. Grant, P. N. Kean, D. Burns, and W. Sibbett, "Passive coupled-cavity mode-locked color-center lasers," *Opt. Lett.*, vol. 16, pp. 384–386, 1991.

[4] U. Keller, W. H. Knox, and H. Roskos, "Coupled-cavity resonant passive modelocked (RPM) Ti:sapphire laser," *Opt. Lett.*, vol. 15, pp. 1377–1379, 1990.

[5] H. A. Haus, U. Keller, and W. H. Knox, "A theory of coupled cavity modelocking with resonant nonlinearity," *J. Opt. Soc. Amer. B*, vol. 8, pp. 1252–1258, 1991.

[6] U. Keller, T. K. Woodward, D. L. Sivco, and A. Y. Cho, "Coupled-cavity resonant passive modelocked Nd:Yttrium lithium fluoride laser," *Opt. Lett.*, vol. 16, pp. 390–392, 1991.

[7] U. Keller, G. W. 'tHooft, W. H. Knox, and T. K. Woodward, "Coupled-cavity modelocking of solid-state lasers using quantum wells," in *Tech. Dig. Quantum Optoelectron.*, 1991, Opt. Soc. Amer., Washington, DC, 1988, pp. 232–235.

[8] H. A. Haus, "Theory of mode locking with a fast saturable absorber," *J. Appl. Phys.*, vol. 46, pp. 3049–3058, 1975.

[9] L. F. Mollenauer and R. H. Stolen, "The soliton laser," *Opt. Lett.*, vol. 9, pp. 13–15, 1984.

[10] K. J. Blow and D. Wood, "Modelocked lasers with nonlinear external cavities," *J. Opt. Soc. Amer. B*, vol. 5, pp. 1228–1236, 1988.

[11] ——, "Mode-locked lasers with nonlinear external cavities," *J. Opt. Soc. Amer. B*, vol. 5, pp. 629–632, 1988.

[12] K. J. Blow and B. P. Nelson, "Improved mode locking of an F-center laser with a nonlinear nonsoliton external cavity," *Opt. Lett.*, vol. 13, pp. 1026–1028, 1988.

[13] P. N. Kean, X. Zhu, D. W. Crust, R. S. Grant, N. Langford, and W. Sibbett, "Enhanced mode-locking of color-center lasers," *Opt. Lett.*, vol. 14, pp. 39–41, 1989.

[14] J. Mark, L. Y. Liu, K. L. Hall, H. A. Haus, and E. P. Ippen, "Femtosecond pulse generation in a laser with a nonlinear external resonator," *Opt. Lett.*, vol. 14, pp. 48–50, 1989.

[15] P. Yakymyshyn, J. F. Pinto, and C. R. Pollock, "Additive pulse mode-locked NaCl:OH$^-$ laser," *Opt. Lett.*, vol. 14, pp. 621–623, 1989.

[16] E. P. Ippen, H. A. Haus, and L. Y. Liu, "Additive pulse mode locking," *J. Opt. Soc. Amer. B*, vol. 6, pp. 1736–1745, 1989.

[17] J. Goodberlet, J. Wang, J. G. Fujimoto, and P. A. Schulz, "Femtosecond passively mode-locked Ti:Sapphire laser with a nonlinear external cavity," *Opt. Lett.*, vol. 14, pp. 1125–1127, 1989.

[18] J. Goodberlet, J. Jacobson, J. G. Fujimoto, P. A. Schulz, and T. Y. Fan, "Self-starting additive-pulse mode-locked diode-pumped Nd:YAG laser," *Opt. Lett.*, vol. 15, pp. 504–506, 1990.

[19] L. Y. Liu, J. M. Huxley, E. P. Ippen, H. A. Haus, "Self-starting additive-pulse mode locking of a Nd:YAG laser," *Opt. Lett.*, vol. 15, pp. 553–555, 1990.

[20] J. M. Liu and J. K. Chee, "Passive mode locking of a cw Nd:YLF laser with a nonlinear external coupled cavity," *Opt. Lett.*, vol. 15, pp. 685–687, 1990.

[21] F. Krausz, Ch. Spielmann, T. Brabec, E. Wintner, and A. J. Schmidt, "Subpicosecond pulse generation from a Nd:glass laser using a nonlinear external cavity," *Opt. Lett.*, vol. 15, pp. 1082–1084, 1990.

[22] G. P. A. Malcolm, P. F. Curley, and A. I. Ferguson, "Additive-

pulse mode locking of a diode-pumped Nd:YLF laser," *Opt. Lett.*, vol. 15, pp. 1303–1305, 1990.
[23] D. E. Spence, P. N. Kean, and W. Sibbett, "60-fsec pulse generation from a self-mode-locked Ti:Sapphire laser," *Opt. Lett.*, vol. 16, pp. 42–44, 1991.
[24] U. Keller, G. W. 'tHooft, W. H. Knox, and J. E. Cunningham, "Femtosecond pulses from a continuously self-starting passively mode-locked Ti:Sapphire laser," *Opt. Lett.*, vol. 16, pp. 1022–1024, 1991.
[25] L. Spinelli, B. Couillaud, N. Goldblatt, and D. K. Negus, "Starting and generation of sub-100 fs pulses in Ti:sapphire by self-focusing," in *Conf. Lasers and Electro-Optics, 1991* (Opt. Soc. Amer., Washington DC, 1991), Postdeadline paper P7.
[26] F. Salin, J. Squier, and M. Piché, "Modelocking of Ti:Sapphire lasers using self-focusing: gaussian approximation," *Opt. Lett.*, vol. 16, pp. 1674–1676, 1991.
[27] N. Sarukura, Y. Ishida, and H. Nakano, "Generation of 50 fsec pulses from a pulse-compressed, cw, passively mode-locked Ti:sapphire laser," *Opt. Lett.*, vol. 16, pp. 153–155, 1991.
[28] N. Sarukura, Y. Ishida, T. Yanagawa, and H. Nakano, "All solid-state cw passively mode-locked Ti:sapphire laser using a colored glass filter," *Appl. Phys. Lett.*, vol. 57, pp. 229–231, 1990.
[29] K. Naganuma and K. Mogi, "50 fs pulse generation directly from a colliding-pulse mode-locked Ti:Sapphire laser using an antiresonant ring mirror," *Opt. Lett.*, vol. 16, pp. 738–740, 1991.
[30] C. Spielmann, F. Krausz, T. Brabec, E. Wintner, and A. J. Schmidt, "Femtosecond pulse generation from a synchronously pumped Ti:Sapphire laser," *Opt. Lett.*, vol. 16, pp. 1180–1182, 1991.
[31] G. Gabetta, D. Huang, J. Jacobson, M. Ramaswamy, E. P. Ippen, and J. G. Fujimoto, "Femotsecond pulse generation in Ti:Al203 using a microdot mirror modelocker," *Opt. Lett.*, vol. 16, pp. 1756–1758, 1991.
[32] U. Keller, W. H. Knox, and G. W. 'tHooft, "Ultrafast solid-state modelocked lasers using resonant nonlinearities," *IEEE J. Quantum Electron.*, invited paper to be published, September 1992.
[33] M. Hofer, M. E. Fermann, F. Haberl, M. H. Ober, and A. Schmidt, "Mode locking with cross-phase and self-phase modulation," *Opt. Lett.*, vol. 16, pp. 502–504, 1991.
[34] G. Gabetta, D. Huang, J. Jacobson, M. Ramaswamy, H. A. Haus, E. P. Ippen, and J. G. Fujimoto, "Femtosecond pulse generation in Ti:sapphire using nonlinear intracavity elements," in *Conf. Lasers and Electro-Opt., 1991* (Opt. Soc. Amer., Washington DC, 1991), Postdeadline paper P8.
[35] W. H. Knox, G. E. Doran, M. Asom, G. Livescu, R. Leibenguth, and S. N. G. Chu, "Low temperature-grown (LT) GaAs quantum wells: Femtosecond nonlinear optical and parallel-field transport studies," *Appl. Phys. Lett.*, vol. 59, pp. 1491–1493, 1991.
[36] U. Keller and T. H. Chiu, "Coupled-cavity resonant passive mode-locked Nd:YLF laser," in *Optical Society of America Annual Meet.*, 1991, paper TuT3.
[37] A. Ashkin, G. D. Boyd, and J. M. Dziedzic, "Resonant optical second harmonic generation and mixing," *IEEE J. Quantum Electron.*, vol. QE-2, pp. 109–124, 1966.
[38] J. Goodberlet, J. Wang, J. G. Fujimoto, and P. A. Schulz, "Starting dynamics of additive pulse mode locking in the Ti:Al_2O_3 laser," *Opt. Lett.*, vol. 15, pp. 1300–1302, 1990, eq. (1).
[39] M. Zirngibl, "High speed photodetectors on strained superlattices," Ph.D. dissertation, No. 854, Ecole Polytechnique Federale De Lausanne, Switzerland, 1990.
[40] T. K. Woodward, T. Sizer II, D. L. Sivco, and A. Y. Cho, "$In_xGa_{1-x}As/GaAs$ multiple quantum well optical modulators for the 1.02–1.07 μm wavelength range," *Appl. Phys. Lett.*, vol. 57, pp. 548–550, 1990.
[41] H. A. Pike and M. Hercher, "Basis for picosecond structure in mode-locked laser pulses," *J. Appl. Phys.*, vol. 41, pp. 4562–4565, 1970.
[42] D. H. Auston, "Higher order intensity correlations of optical pulses," *IEEE J. Quantum Electron.*, vol. QE-7, pp. 465–467, 1971.
[43] For example A. E. Siegman, *Lasers*. Mill Valley, CA: Univ. Sci. 1986, ch. 27.5, p. 1090.
[44] A. A. Kaminskii, *Laser Crystal, their Physics and Properties*. New York: Springer-Verlag, 1981.
[45] M. C. Nuss, U. Keller, G. T. Harvey, M. S. Heutmaker, and P. R. Smith, "Amplitude noise reduction of 50 dB in colliding-pulse mode-locking dye lasers," *Opt. Lett.*, vol. 15, pp. 1026–1028, 1990.
[46] U. Keller, K. D. Li, M. Rodwell, and D. M. Bloom, "Noise characterization of femtosecond fiber raman soliton lasers," *IEEE J. Quantum. Electron.*, vol. 25, pp. 280–288, 1989.
[47] H. A. Haus, "Parameter ranges for CW passive mode locking," *IEEE J. Quantum Electron.*, vol. QE-12, pp. 169–176, 1976.

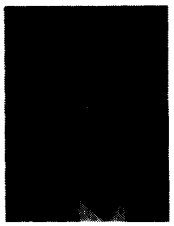

Ursula Keller (M'89) was born in Zug, Switzerland, in 1959. She received the "Diplom" in physics from the Federal Institute of Technology (ETH) Zürich, Switzerland, in 1984 and the M.S. and Ph.D. degrees in applied physics from Stanford University, Stanford, CA, in 1987 and 1989, respectively. Her Ph.D. research was in optical probing of charge and voltage in GaAs integrated circuits and in low-noise ultrafast laser systems.

From late 1984 to 1985 she worked on optical bistability at Heriot-Watt University, Edinburgh, Scotland. In 1989, she joined the AT&T Bell Laboratories, Holmdel, NJ, as a member of the technical staff where she conducts research on photonic switching, ultrafast laser systems, and semiconductor spectroscopy.

Dr. Keller is a member of the Optical Society of America. During 1985–1986 she was a Fulbright Fellow and in 1987–1988 she received the IBM Predoctoral Fellowship.

T. Heng Chiu was born on May 2, 1953, in Hong Kong. He received the B.S. degree in physics from the National Taiwan University, Taipei, Taiwan, in 1976. He served in the Marine Corps of the Republic of China for two years, and then received his M.S. and Ph.D. degrees in physics from the University of Illinois, Urbana-Champaign, in 1980 and 1983, respectively. His doctoral work concerned the core level excitations in alkali metals and alloys.

In 1983, he joined the AT&T Bell Laboratories, Murray Hill, NJ, for his post-Doctoral research in molecular beam epitaxy. Since 1985, he has served as a staff member with Bell Laboratories, Holmdel, NJ, where he continued his research on chemical beam epitaxy and molecular beam epitaxy of III–V semiconductor materials, and their optoelectronic device applications. He has published over 100 papers in the areas of optoelectronic materials and condensed matter physics.

Dr. Chiu is a member of the American Vacuum Society.